Effect of beam web bolt arrangement on catenary behaviour of moment connections

Effect of Beam Web Bolt Arrangement on Catenary Behaviour of Moment Connections

Ling Li [2],Wei Wang *[1, 2], Yiyi Chen [1, 2], Yong Lu [3]

[1]*State Key Laboratory of Disaster Reduction in Civil Engineering, Tongji University, Shanghai 200092, China*

[2]*Department of Structural Engineering, Tongji University, Shanghai 200092, China*

[3] *Institute for Infrastructure and Environment, School of Engineering, The University of Edinburgh, Edinburgh EH9 3JL, UK*

Abstract: In a column-removal scenario for a building structure, the catenary action will play an essential role for the frame in resisting a progressive collapse. This paper investigates the catenary behaviour of welded unreinforced flange - bolted web connection (i.e. WUF-B connection) connections in plane frames by means of full-scale testing and numerical simulation. Two different layouts of bolts at the beam web were considered, with four bolts arranged in one row or two rows in the two specimens, respectively. The results demonstrate that both specimens of the WUF-B moment connection were able to develop an effective catenary action via the bolted web following the primary flexural phase. The failure modes of the bolted web vary with different bolt arrangements under the catenary action. When all (four) bolts were arranged in one row, the lowest bolt bearing area on the web tends to be compressed to fracture before bolt tear-out failure occurs near the weld access hole. When the bolts were arranged in two rows, however, the shear tab cracked at the section across the bolt holes. The former failure mode is deemed to be more robust than the latter under a column removal scenario.

Keywords: progressive collapse; catenary action; WUF-B connection; experiment; numerical simulation; bolts; fracture.

---

* Corresponding author. Tel.: +86-21-65982926; Fax: +86-21-65984976.
Email address: weiwang@tongji.edu.cn (W. Wang)

1. Introduction

As a general guide to preventing disproportionate or progressive collapse in the event of a critical local failure, a structure should be designed to possess an adequate degree of continuity and ductility, in addition to strength [1-3]. As far as a frame structure is concerned, the structural system should be able to bridge over the failed load-carrying member, particularly a failed column. Moment-resisting beam-column connections, which hold the critical path of the gravity load in a framed structure, are generally beneficial in terms of the structural redundancy [4]. After the removal of a column, a “double-span” scenario arises, and the soundness of the affected moment connections will play a central role in withstanding and redistributing the gravity loads from the upper storeys over the emerged double-span [5-11]. In this process, the connection(s) and the adjoining members will typically experience an intensified flexural action stage, followed by a catenary action phase as the deflection in the double span becomes large.

It has been demonstrated [11-17] that the catenary action mechanism has the potential to considerably supplement and eventually replace the flexural action in carrying the vertical load. However, it can be understood that the realisation of an effective catenary action depends upon two basic conditions, a) a sufficiently large axial tension can develop in the beams, and b) such axial tension can maintain while large deformation (and hence large slope) advances, which would effectively enable the transfer of the vertical load via the axial tension of the beams to adjacent columns. In this respect, the ability of the connections in withholding a necessary degree of integrity into the large deformation regime becomes critically important.

According to the preceding experimental investigation of beam-to-tubular column moment connections under the column removal scenario [17], different connecting methods at the web may provide a similar flexural capacity but they could end up with considerably different catenary action capacity after flexural failure occurred. For a welded-web connection, the flexural action and catenary action mechanisms tend to deteriorate simultaneously because of continuous crack propagation after the bottom flange of the beam section fractured. In contrast, a bolted web connection enables the catenary action to develop more effectively, thanks to the interaction of the beam web with the bolts and shear tabs even after fracture occurs in the bottom flange. In another experimental study on the bolted web connections under a column removal scenario conducted by Sadek [12], the loading capacity was observed to reduce following the fracture of the bottom flange near the weld-access hole. Unfortunately the test terminated

shortly after the bottom flange fractured, so the performance of the moment connection in the catenary phase could not be examined.

This paper investigates the catenary behaviour of the typical H-beam and square-column moment connections with a bolted web connection, with a particular focus on the influence of different bolt layouts on the structural resistance in the large deformation regime. Two full-scale beam-to-column assemblies with welded unreinforced flange - bolted web connection (i.e. WUF-B connection) were designed in detail in accordance with a prototype steel building frame, and they were constructed and tested under a push-down action applied at the unsupported center column location. The experimental results are presented and discussed comprehensively. In conjunction with the experiments, numerical simulations with a detailed finite element model incorporating material fracture are conducted to verify the load transfer and failure mechanisms of the WUF-B connections, especially in the catenary response phase.

2. Experimental programme

2.1. Test specimens

The test specimens were designed to represent the beam-to-column connection region in a column removal scenario. For this purpose, a Beam-Joint-Beam (B-J-B) assembly is considered appropriate [17]. Such an assembly, as depicted in Fig. 1, is extracted from the directly affected spans of the frame when a middle column is removed, assuming that the inflection point is located around the mid-span of the original beam members in such a scenario. This configuration allows the full details at the connection to be reproduced, while the column removal scenario can be simulated by a push-down action via a center column, as will be shown in Section 2.2.

The WUF-B connections between the H-beam and the square hollow section (SHS) column are investigated in this paper. The geometrical characteristics of the assemblies are given in Table. 1. The main difference between the two test specimens under consideration, namely SI-WB and SI-WB-2, lies in the arrangement of the web bolts. The span of the beam is l_0 = 4500mm (giving a gross span-to-depth ratio of l_0/H = 15), and the height of the center column is 1100mm, as will be illustrated later in the test set-up. The design of the beam-to-column assemblies was made following a strong column - weak beam seismic design philosophy and specific requirements in Chinese codes [18, 19].

Fig. 2 illustrates the details of the connections. In each specimen, two H-section beams were connected to the SHS column via the WUF-B connection, and within the joint region two inner-diaphragms were installed inside the column at the locations corresponding to the top and the bottom flanges of the beam. It is worth noting that such a connection configuration with internal diaphragms in a square tubular column is commonly used in steel construction to maintain the column continuity and at the same time to ensure sufficient beam-to-column joint flexural stiffness [20, 21].

The flanges of the beam, as well as the inner-diaphragms inside the column, were jointed to the column wall using complete joint penetration (CJP) groove welds, and weld access holes of the beam were cut from the beam web in accordance with a standard recommendation [22]. The beam was bolted on the web to a shear tab which was pre-welded to the column, via four M20 Grade-10.9 frictional type high-strength bolts. Four bolts were arranged with two different layouts in the two specimens; Specimen SI-WB had all four bolts arranged in a single row along the depth of the web (see Fig. 2 (a)), whereas Specimen SI-WB-2 had the four bolts arranged in two rows around the mid-height region of the web (see Fig. 2 (b)). The pre-tightening force and torque applied on the bolts were 155 kN and 440 N-m, respectively, according to standard requirements [23]. All the contact surfaces were pre-treated with sand blasting. The measured material properties of the SHS column and the H-section beams are summarized in Table 2.

2.2. Test setup

A purpose-built test setup was employed for the series of tests, as schematically illustrated in Fig. 3. The test specimen was supported by a horizontally self-balanced support frame, while the vertical load was supported by a vertical reaction frame mounted on the strong floor.

The test specimens were loaded vertically at the top of the center column to simulate the effect following the removal of the middle column below. To avoid complication in the loading condition, the center column was guided at the bottom end using a sliding support so that only vertical movement was possible. This configuration effectively simulates a symmetrical condition which is considered representative in a building collapse scenario (see Fig. 1 of the paper) and it also allows a simpler setup for the application of the pushdown load from the top of the column. The sliding support at the column bottom end consists of an interior connector and a rigid exterior guiding box, and the interior connector is made of multiple ball-joints arranged around the connector. As the connector

is ball-jointed, the friction incurred during the tests was negligible and this was confirmed by checking the applied load with the internal forces obtained from analyzing the measured strains, as described in Section 4.4. The specimens were pin-supported at the two horizontal ends with latch-type rollers to realise free rotation at the beam ends within the test plane. The tightness and stiffness of the pin supports were assured by using a manufactured strong pin joint connected to the support frame, as illustrated in Fig.3. The pin joint actually allowed slight horizontal adjustment so as to cater to any imperfection in the setup, and any displacements that occurred at the pin joint during the tests were measured by the transducers. The distance between the two pin supports was 4500mm. The vertical load was applied in a quasi-static manner with a displacement rate of less than 7mm/min during the tests. The test was terminated once the maximum vertical displacement at the central column was reached.

As depicted in Fig. 4 (a), due to the top and bottom constraint of the centre column in the test, a symmetrical assembly is supposed to deform as two independent half parts under the vertical load. It is also acknowledged that, in a column removal scenario for an actual building (refer to Fig. 4 (b)), the constraint at the bottom of the assembly would not be provided. Nevertheless, as observed in relevant test findings [12, 17], the entire assembly still symmetrically carries the upper load prior to the first occurrence of a severe damage (for instance the fracture of beam bottom flange). Thereafter, the column would suffer an unbalanced action as a result of the different resistances of the intact or damaged connections on both sides. Therefore, a certain amount of column slope may be induced and its magnitude is believed to depend upon the flexural stiffness of the column. The influence of such column slope on the response of the assembly during the whole loading process will be assessed in Section 4.5 by the means of the detailed finite element analysis. The analysed assembly consists of a one-storey-height column and two connected beams as shown in Fig. 4 (b), and the connection configuration is identical to that of Specimen SI-WB-2. From the analysis results, the one-storey-height column generally kept vertically moving and the response of the assembly agreed with the simulation results of the Specimen SI-WB-2. In view of this, the response of the assembly in the experimental boundary condition (refer to Fig. 4 (a)) could represent the situation in an actual building (refer to Fig. 4 (b)).

Furthermore, the sliding support at the bottom of the centre column is significant for securing the loading apparatus. As depicted in Fig. 5, in the case without bottom constraint the bottom of the column, a considerable bending moment due to the unbalanced axial

forces in the beams generates at the top of the column and makes the connected loading apparatus at risk of being damaged. Thus it is a good solution by constraining the bottom end of the column to balance the additional moment at the top, as employed by Yang [14, 15].

2.3. Instrumentation

Instrumentation was arranged to measure the distribution of displacements along the length of the beam and strains at the critical regions during the tests. Fig. 6 shows the instrumentation arrangement in the two tests.

As can be seen from Fig. 6 (a), as many as 18 transducers were used to measure the deflection of the beam-to-column assembly along the beam length and any possible movements of the two pin support rollers.

More than 100 strain gauges were used to measure the strains at critical locations on the column wall and at selected sections of the beams, with an overall arrangement as illustrated in Fig. 6 (b), while the detailed arrangement of these strain gauges can be found in Fig. 6 (c) and (d) for Specimen SI-WB and Specimen SI-WB-2, respectively. Due to the stiffening effect of the weld on the sections that connected the beam members to the column wall, the nearby Sections W3 and E3 were expected to represent the most critical sections in the beam-to-column assembly under the column removal scenario. The anticipated large strains at the flanges of Sections W3 and E3 were measured by special strain gauges with an effective range of more than 100,000 με.

It is noted that the strains on the Sections W1 and E1 of the beam members (see Fig. 6 (b)), where only elastic response was anticipated, were measured to allow for a calculation of the internal forces at these sections, and hence a deduction of the reaction forces at the pin supports.

3. Experimental results

3.1. General behaviour and failure modes

The measured relationships of the vertical load versus vertical displacement at the center column location from the two tests are shown in Fig. 7. A few key stages of the response are identified on the curves, and the associated damage developments are depicted in the corresponding photographs included in Fig. 8. It is noted that a nominal plastic load, F_p, is

employed for the normalisation of the applied load. F_p is calculated as the vertical load corresponding to the state where the full plastic yield moment of the beam section was achieved at the critical location (Sections W3 and E3), and it is found to be 180kN in both specimens. The beam chord rotation θ is evaluated by dividing the applied displacement at the center column by the distance between the centerline to the pin support (effectively half-span length) of 2.25 m.

In the SI-WB specimen (see the black curve in Fig. 7 and the photographs in Fig. 8 (a)), the first significant failure event (point "A1" on the load-displacement curve) took place when local buckling occurred at top flanges near Section W3 and E3, while the displacement reached about 110mm, which corresponded to the beam chord rotation θ of 0.048 rad. After that, the development of sliding between the bolts, webs and shear tabs was evident and even the sound of bolt sliding was continuously heard from the test. The specimen reached a peak load (point "A2") when the bottom flange (near the weld access hole) at Section E3 fractured, and the corresponding displacement was 234 mm (θ = 0.104 rad). The fracture caused a steep drop of the force from the peak load of 275 kN (1.54F_p) to 122 kN (0.68F_p). The specimen then saw a gradual pick up of the vertical force, showing an apparent change of the resistance mechanism to a catenary-action dominated regime. Meanwhile at the lower bolts of Section E3 large bearing deformation occurred on the web with the bolt holes deforming into elliptical shapes. Eventually at the center displacement of 345 mm (θ = 0.153 rad), bolt was torn out of the web across the lowest bolt hole and the nearby weld access hole (point "A3"). The test was terminated at this point, and the vertical force had reached 306 kN (1.70F_p), which exceeded the earlier peak value and was still in an increasing trend.

In the SI-WB-2 test (see the grey curve in Fig. 7 and the photographs in Fig. 8 (b)), the load-displacement development path was identical to that of test SI-WB in the early stage, with the failure initiated from local buckling at top flanges near Section W3 and E3 (point "B1"). The load still kept increasing until the column wall cracked near the bottom flange on the west side (point "B2") when the displacement reached 137 mm (θ = 0.061 rad), at which stage the load dropped abruptly from 207 kN (1.15F_p) to 158 kN (0.88F_p). The rotational constraint exerted by the centre column effectively allowed the bending strength of beam on the other side (east side) to continue developing until the bottom flange (near the weld access hole) at Section E3 fractured (point "B3"). At this point the flexural capacity of the system effectively lost altogether, causing a steep drop of the load from 226kN (1.26F_p) to only 57 kN (0.32F_p). The corresponding displacement was 243 mm (θ =

0.108 rad).

With further increase of the displacement, the load gradually picked up at a similar rate as in specimen SI-WB, apparently due to the development of the catenary effect. As a result of large deformation, the crack of the column wall on the west side propagated across the entire width of the bottom flange. The column wall fractured completely across the thickness (point "B4") when the displacement reached about 316 mm (θ = 0.140 rad), and this was accompanied with a slight dip of the load from 180kN (1.00F_p) to 150 kN (0.83F_p). Thereafter the west-side column wall tore up from the two ends of the bottom fracture line; however the vertical resistance was able to increase persistently thanks to the catenary action. Eventually the shear tab cracked vertically through the bolt holes at Section E3 (point "B5"), but the load kept increasing even when the displacement reached 387 mm (θ = 0.170 rad). The test was terminated at this point, and the vertical load had reached 232 kN, or 1.29F_p which exceeded the maximum load level reached during the flexural phase of the response.

The failure process in the two specimens shared some general commonalities. In both cases the process may be divided into three distinctive phases, namely a flexure-dominated phase, a flexure-to-catenary transitional phase and a centenary action dominated phase. The transitional phase in both cases came to an end (point A2 for SI-WB and point B3 for SI-WB-2) at about the same level of the vertical displacement, which was around 240mm or 0.1 rad. Whether or not the flexural phase would involve a marked interim stage as evidenced in Specimen SI-WB-2 would depend upon the development of flexural failure in the beams of the two sides and the effectiveness of the rotational constraint exerted by the centre column. However, the severity of the flexural failure tended to have a significant effect on the magnitude of decrease in the vertical load, which in turn affects the vertical load carrying capacity during the catenary action phase for a comparable level of deformation. In the two specimens under consideration, the load carrying capacity in SI-WB-2 was generally lower than that in SI-WB by about 35% in the catenary phase of the response.

Whereas flexural failure occurred in the critical beam regions in both specimens, specimen SI-WB-2 exhibited a more complex failure process and it also involved local failure (fracture) in the column wall. Close inspection revealed that the bottom inner-diaphragm within the column connection region had separated, as shown in Fig. 9, thus the column wall had to transfer the tension force of the beam bottom flange, leading to large local deformation and eventually fracture in the column wall. It should be noted

that such a local failure mechanism to the column wall could vary and be prevented altogether depending upon the quality control of the welding. In view of this, further discussion will be focused only on the failure to the most critical beam section with single- or two - row bolt layout.

Since the bottom end of the centre column was guided to move only vertically, the rotational freedom at the connection was minimal; consequently the response of the assembly on one side of the column affected little that of the other side. This condition, which represents an upper bound rotational constraint at the connection, effectively allows both sides of the connection to eventually develop their full capacities, albeit one after the other. As a representation, the east side of the assembly, which did not involve a weld failure at the column internal diaphragm and hence exhibited a more stable response, will be examined in more detail.

Overall, both specimens were able to transit into an effective catenary action following the end of the primary flexural phase, which was marked by fracture at the bottom flange. Such a degree of resilience of the WUF-B connections was apparently attributable to the robustness of the connection mechanism via the bolts while the structure underwent excessively large deformations. This observation echoes the findings from testing a pair of tubular connections where bolted and welded joints were used respectively [17], and it further suggests that a bolted connection is generally favourable for steel frames in resisting progressive collapse.

3.2. Deformation shapes and limit displacements

The shift from a flexural mode of response to a tension-catenary mechanism can be further observed from the change of the deflection shapes in the specimens, as depicted in Fig. 10 for Specimen SI-WB. The deflected profiles exhibited a typical flexural pattern at the early stages of the response. As the deflection increased, the deformation became increasingly concentrated at the connection, and eventually turned into a profile that resembled two straight lines (the beam member) connected to the center column like a hinge. A similar development of the overall deformation was observed in Specimen SI-WB-2, with its permanent deformation pattern shown in Fig. 11.

For general applications, it would be instructive to identify the characteristic deformation limits, as well as the relative peak loads, from the experiments. The results for the two test specimens are summarized in Table 3. Specimen SI-WB-2 exhibited two peak loads as a result of the bending - tension combined failure occurring on each side of the

column one after the other at distinctive deformations, while Specimen SI-WB was dominated by the response on one (east) side of the assembly.

From the test data in Table 3, the peak loads in the primary flexural phase were all greater than the theoretical full-plastic load F_p, and this indicates that the flexural capacity in both specimens was well developed before the critical bottom flange fractured The primary flexural phase apparently ended in both specimens at about the same deflection limit of approximate 0.1 rad in terms of the chord rotation. After a steep drop of the load, the vertical resistance was able to pick up persistently in the catenary phase, and at about a beam chord rotation of more than 0.15~0.17 rad the vertical load capacity exceeded the flexural peak load.

3.3. Strain evolution and distributions

Fig. 12 depicts the strain development at the "elastic" Section E1 with the increase of the deformation in terms of the beam chord rotation. All strains were indeed less than the yield strain of 2×10^{-3}, as expected, and therefore can be used to calculate the internal forces within the section and subsequently throughout the entire assembly.

From Fig. 12it can be seen that when the beam chord rotation was less than 0.03 rad, these beam sections behaved primarily in flexure with the top flange in compression and the bottom flange in tension. The centroid axis located slightly above the mid-height of the web, indicating the presence of certain axial tension. Beyond the beam chord rotation of 0.03 rad and prior to the bottom flange fracture at about 0.10 rad, all strains tended to increase more or less uniformly, signifying a transition from bending to a bending - tension combined response. In the process, the strains in Specimen SI-WB-2 dropped temporarily when the column wall cracked on the west side (point "B2"). After the fracture of the bottom flanges at the critical beam regions (point "A2" and "B3"), the strains at locations farther away from the centroid (especially towards the bottom flange) dropped significantly as a result of an abrupt reduction in the bending action. The whole section was under tension in the catenary phase, despite that certain variation existed among different locations across the section depth.

Fig. 13 plots the strain distributions of Section E2, which was adjacent to the critical Sections E3, up to the fracture of the bottom flange. Note that some data points are missing because of damage to the corresponding strain gauges. It can be observed that Section E2 also exhibited clear flexural behaviour in the early stage of the response (up to a displacement of about 50mm). With increased loading, the tensile strains at the bottom

flanges and compressive strains at the top flanges grew rapidly because of large plastic deformation. At the later stage the deformation was overwhelmed by the plastic strains, with the maximum strain values exceeding 0.03% before the bottom flanges fractured. This indicates that the critical section was able to achieve almost full plasticity at the verge of the flexural failure.

4. Numerical Analysis with fracture simulation

A numerical simulation study using a refined finite element model has been conducted. The main objectives of the numerical study are three folds, a) by comparing with the experimental results, to verify and validate the FE model, particularly with regard to the simulation of fracture and its effect on the global behaviour; and b) using the validated model to assist in interpretation of the experimental results and exploration of the failure mechanisms in detail; c) using the validated model to investigate and assess the effect of the boundaries on the performance of the assembly.

The numerical analyses were carried out using the explicit time integration approach in the general-purpose finite element analysis software ABAQUS [22]. The developed FE model took into account geometrical, boundary and material nonlinearities, as well as fracture, in the analysis. The load was applied by pushing down the central column stub under a displacement-controlled scheme with a sufficiently slow rate to ensure that no inertial effect is involved.

4.1. Basic modeling considerations

Each test specimen was modeled in its entirety as illustrated in Fig. 14 (a), so that a non-symmetrical development of damage process may be incorporated. All parts in the assembly were modeled using solid elements, covering the beam and column components, as well as essential connection details including inner-diaphragms, shear tabs and bolts. The details of welds were not considered as failure will be governed by the adjacent material. The interface between the bolts and the web walls and shear tabs was defined by Contact with nominal friction. As shown in Fig. 14 (b) ~ (d), sufficiently fine mesh of solid elements was employed in the connection zone where fracture may occur, with a size of approximately 1.0 mm.

4.2. Material models and fracture simulation

The actual material coupon test results (Table. 1) were used in defining the stress-strain

constitutive relationships, including the fracture strain limits. To simulate the fracture in the steel, the “Damage for Ductile Metals” approach is employed, such that individual elements would be deleted once their strain response reaches the pre-specified fracture threshold [24].

Particularly, in order to capture the local failure of the column wall on the west side in Specimen SI-WB-2, it is necessary to reproduce the separation between the bottom inner-diaphragm and the column wall in the test (refer to Fig. 9). For this purpose, special meshes were set at the western part of the bottom inner-diaphragm, whose material possessed a relatively small fracture strain limit. Thus this part could fracture in advance simulating the separation as stated above, which is a precondition for the subsequent fracture of the adjacent western column wall.

4.3. Failure modes and load-displacement relationships

The failure patterns from the FE simulation are shown in Fig. 15, to compare with the corresponding experimental results presented earlier in Fig. 8. Similar to the observation from the experiment, the FE model SI-WB fractured at the bottom flange of Section E3 (see step “a2” in Fig. 15 (a)). Thereafter, the bending effect is transferred mainly via the bolts, and this causes compressive stress in the bolt bearing area within the web, resulting in bearing damage in the web and subsequently bolt tear-out failure (step “a3”). In Specimen SI-WB-2, fractures at the column wall and Section E3 that occurred in the experiment were also reproduced in the FE model. On the west side of the assembly, the crack initially took place between the bottom inner-diaphragm and the column wall (step “b2i” in Fig. 15 (b)), causing subsequent crack at the adjacent column wall (step “b2ii”) and the final through-thickness fracture (step “b4”). At Section E3 on the east side, fracture occurs firstly at the bottom flange of beam member (step “b3”) and then at the shear tab section across the bolt holes inside (step “b5”).

Fig. 16 compares the relationships of vertical load versus displacement at the central column from numerical simulation with the tests results, where the key damage events are marked in accordance with those depicted in Fig. 8 and Fig. 15. The comparison shows a favourable agreement in terms of the development of the resistance and the evolution of damage. Generally speaking, the vertical resistance of the assembly from the numerical simulation is greater than the experimental result, particularly in the later stage after the fracture occurrence. This is not supervising given the severity of the local damage involved.

It is noted that in the simulation for Specimen SI-WB-2, the load dropped abruptly when the inner-diaphragm fractured and separated from the column wall on the west side (step "b1i"), but then immediately recovered to the previous value. Such a phenomenon is understood to have arisen from numerical fluctuation due to a significant sudden disturbance of the equilibrium state, and hence may be ignored.

4.4. Internal force development at the critical beam section

The relative significance of the bending moment and the axial force is representative of the change of the resistance mechanisms. As mentioned in Section 3.3, in the experiment the internal forces were deduced from the elastic strain measurement at sections near the supports. **A** detailed description of how to determine the internal forces [17] can be referred to. In this section, the results are solely based on the east (right) side of each assembly, which does not involve any weak weld material assumption. As a matter of fact, because of the enforcement of symmetry along the central column (see Fig. 4(a)), which is also replicated in the FE model, the behavior of each side of the assembly was effectively independent from the opposite side. Therefore, the comparative results on the bolt layouts are valid. Fig. 17 shows the development of the bending moment and axial force at the critical Section E3 from the FE analysis as compared with the experimental results. In the plots, the axial force N is normalised by the full plastic tensile capacity of the cross section, N_p (N_p = 1641 kN), and the bending moment M is normalised by the full plastic flexural capacity M_p (M_p = 188 kN-m). As can be observed, the numerical and experimental results agree well with each other.

The bending moment-displacement curves exhibited a usual flexural behaviour during the flexural phase of the response encompassing elastic and nonlinear plastic stages until the bottom flanges fractured. With the fracture of the bottom flange, the bending moments dropped abruptly, and then further decreased to virtually zero and even into the negative region in the final stage. On the other hand, the axial tension generally increased as the plastic bending deformation accumulated, leading to a persistent increase of the vertical resistance (refer to Fig. 16 (a)), despite an almost flat sectional bending moment. The fracture of the bottom flange caused a temporary drop of the axial tension, but it immediately recovered, and thereafter kept increasing to become the primary resistance mechanism in the catenary-dominated phase. In the final stage, the axial tension reached a maximum value of about $0.6N_p$.

4.5. Effect of the constraint at the bottom of the centre column

As depicted in Fig. 3, the bottom of the specimen assembly is rotationally and horizontally constrained by the sliding support, which is artificially designed for a secure loading in the experimental research. Although the bottom of the column would become unconstrained once the column part below is removed in an actual building, a column with sufficient stiffness may generally maintain a vertical movement during this process.

In this section, an additional analysis was conducted to assess the effect of the constraint at the bottom of the specimen on the response of the beam-to-column assembly. Result comparisons would be made between the finite element models of two similar beam-to-column assemblies with the same connection configuration and material models but with different boundary conditions of the centre column. One was exactly the test specimen assembly ((refer to Fig. 4 (a)) as stated in last sections. The other one was modelled on the basis of the former assembly but extending the column up to the upper storey (suppose the storey height h_0= 3m) and making the bottom of the centre column unconstrained (refer to Fig. 4 (b). The top of the one-storey-height column was rotationally and horizontally constrained to simulate the boundaries provide by the connected beams and the floors of the upper storey. Taking the connection configuration of Specimen SI-WB-2 for example, Fig. 18 compares the vertical resistances of the assembly between two models, which are labeled as ‘with bottom constraint’ and ‘without bottom constraint’, respectively. As can be seen, the two assemblies performed consistently with each other, because the columns could keep vertically moving with increasing displacement in two models. Thus it is implied that, the constraint at the bottom provided by the sliding support in the test is of little influence on the resistance of the connection for preventing progressive collapse. In other words, for an experiment research aiming to study the robustness of the connection, either a sufficient rotational constraint at the top of the column (as employed by Sadek [12]) or a constraint at the column bottom (as employed by Yang [14, 15] and Li [17]) should be set up to keep a smoothly vertical movement of the column in the loading process.

5. Performance of bolted web connection under catenary action

The WUF-B connection has been experimentally proven to be generally effective in facilitating the development of the catenary action after a flexural failure. Nonetheless, the actual efficiency of a particular WUF-B connection is still dependent upon the detailed arrangement of the bolts across the web. The influence of the bolt layout is further

discussed with the aid of the FE analysis in this section.

5.1. Contribution to the force transfer in different phases by the bolted web

In the flexural phase, the beam-to-column connection primarily relies on the top and bottom flanges to resist the bending moment, whereas the web connection zones with different bolt layouts play a relatively insignificant role. This is evidenced from very similar load-deflection curves in the first stage of the response in Fig. 7. Once the critical section fractures at the bottom flange, its flexural capacity drastically deteriorates. Henceforth, the force transfer mechanism shifts from a flexural mechanism to a catenary mechanism, with the axial force becoming a dominant factor.

With the fracture of the bottom flange, the bolted web becomes the key to the development of the catenary action as well as the residual bending capacity. Fig. 19 shows the stress and strain distributions over a cross-section in the close vicinity of the bolted area from the numerical simulation for the two specimens; the plots of stress and strain in the post-fracture phase are indicated in dashed line. Before the bottom flange fractures (with a central deflection below about 200 mm), the stresses and strains of the web in Specimen SI-WB were greater than those in Specimen SI-WB-2, indicating a larger contribution in the bending resistance from the web when all the four bolts were arranged in a single row. In the post-fracture stage, the stresses and strains of the residual section distributed in a more uniform manner over the entire web depth in Specimen SI-WB than in Specimen SI-WB-2, once again indicating a more efficient participation of the bolted web in the one-row bolt arrangement.

5.2. Effects of bolt layout on the failure modes at the web

It has been observed from the tests and the numerical simulations that the bolt layout at the web of WUF-B connection markedly affects the force transfer after fracture at the bottom flange. Fig. 20 further compares the engagement of the bolted web and the sequence of the failure in the bolt bearing areas between the two bolt arrangements based on the FE analysis. Within each layout scheme there is always scope for improved performance by enhancing the weak links under each scheme, and this falls into the area of detailing enhancement and optimization involving many factors such as plate size, plate thickness, edge distances and the height of the shear tab etc. The results presented in this section would help set out a general direction.

With all the bolts arranged across the depth of the web in one single row such as

Specimen SI-WB (Fig. 20 (a), the lowest bolt area is subjected to the severest stress after the bottom flange fracture (point “0”) occurs; as a result, the bolt bearing wall undergoes a compression failure (point “1”) and this is followed by a bolt tear-out failure of the web near the weld access hole (point “2”). A similar stress condition and potential failure then shifts upwards to the next bolt (point “3”), and so forth. Understandably, the bolt tear-out failure of the web could be prevented if the distance from the bolt holes to the edge of the connected components is made sufficiently large (certainly larger than in specimen SI-WB).

When the bolts are arranged in two (or more) rows located around the middle part of the web, such as in Specimen SI-WB-2 illustrated in Fig. 20 (b), the much narrowed shear tab section could turn to be the weakest link, leading to rupture of the shear tab across the bolt holes in a progressive manner starting from the lower bolt upwards. When the shear tab ruptures completely (across points “1” to “3”), the beam will be tied to the column merely by the top flange, which would provide little tensile capacity for the assembly and therefore constitute a complete failure. The damage pattern is featured by the plate crack at the net section, whose section area may be too small to provide a sufficient capacity.

With respect to the associated deformability during the failure process, the failure mode featured by the compression of the bolt bearing area tends to be more ductile than the case involving rupture of the connection plate. From the observations outlined above, it is reasonable to deduce certain measures about the configuration at the bolt connection region to improve the robustness of the WUF-B connections. Clearly, allowing a sufficient distance between the bolt holes and the edge of the connected components would effect to postpone or even avoid bolt tear-out failure, see the improvement drawing in Fig. 20 (a). On the other hand, enlarging the cross section of the connection plate (shear tab) could prevent the rupture of the plate and therefore allow for a ductile failure mode to develop (Fig. 20 (b)).

5.3. Simulation of the response of the assembly into final failure

In the experiment the two specimens were tested into advanced catenary action, but they were not completely failed due to the limited displacement range of the test setup. In this section, the FE model was employed to analyse the entire response process until the eventual failure stage. For simplicity, each FE model herein consisted of just a half of the assembly with a symmetrical boundary imposed along the centerline of the column, as depicted early in Fig. 4 (a). Other details of the FE model and the material models

remained the same as those used in the experimental verification, except that this model does not involve any weak weld material assumption. The results of the development of the normalised internal forces at the critical section E3 in the two models are illustrated in Fig. 21.

The development of the bending moment and axial force through the flexural failure at about 200mm and up to an advanced catenary action of around 350mm (end of the experiments) was similar to the comparison shown in Fig. 17. With further increase of the deformation, the axial tension of Specimen SI-WB maintained until a central displacement of approximately 430mm (0.19rad). In comparison, the axial tension in Specimen SI-WB-2 was on a decreasing trend due to the continuous crack at the shear tab when the displacement exceeded 310mm, showing a less ductile behaviour with a smaller tensile capacity.

The vertical resistance of the FE models is plotted against the increased displacement in Fig. 22. It can also be seen that the two cases result in a similar response in the flexural phase, but marked differences in the catenary phase. Relatively speaking, SI-WB outperformed Specimen SI-WB-2, especially in the catenary phase.

6. Conclusions

Full-scale experimental studies have been conducted to investigate the behaviour of WUF-B type of steel moment connections with an inner-diaphragm under a column removal scenario, with a particular focus on the effect of different layouts of the bolts. Two beam-column assemblies were designed, constructed and tested, one with all four bolts at the connection arranged in a single row across the beam web, and the other with the bolts arranged in two-rows around the middle portion of the beam web. Numerical simulation with detailed finite element models for the two test specimens has also been carried out to further study the failure modes of the bolted connections.

The two cases with different bolt layouts exhibited almost identical response until the bottom flange fractured, which signified the end of the flexural action phase. The design with all bolts arranged in a single row over the entire web area (Specimen SI-WB) was able to engage the beam web into action more effectively after the bottom flange failure, allowing for a smoother transition into the centenary action phase than the case with the two-row layout of the bolts (Specimen SI-WB-2).

The finite element model incorporating the feature of fracture simulation was capable of reproducing the transition of the resistance mechanisms and the failure modes. The model

provides further information about the local failure sequences and can be employed for extended parametric calculations. Assisted by the validated FE models, the effect of the bottom constraints of the centre column on the assembly was assessed and results confirmed that the boundaries of the test specimens generally accord with those in an actual building after a centre column removal.

In general the bolted connections have been shown to be robust in withstanding large deformations while the resistance mechanism transitioned to a catenary action phase. Relatively speaking, a single-row bolt arrangement has inherent advantage over the two-row arrangement (of same total number of bolts) and this is determined by the force transferring efficiency under bending and the subsequent knock-on effect when moving into the catenary action regime. Scrutiny of the local failure patterns indicate that further improvements in both cases may be achieved by enhancing the local connection details, in particular a safeguard of the bolt bearing capacity by ensuring a sufficient distance from the bolt holes to the end surface of the beam, and the prevention of the shear tab rupture by enlarging the section of the connection plate. More specific guides to the design and optimization of such details warrants further parametric analysis and this will be addressed in subsequent studies.

Acknowledgments

The research presented in this paper was supported by the Natural Science Foundation of China (NSFC) through Grant No. 51008220 and the Ministry of Science and Technology of China through Grant No. SLDRCE09-B-02. Any opinions, findings, conclusions, and recommendations expressed in this paper are those of the authors and do not necessarily reflect the views of the sponsors.

References

[1] General Service Administration: Progressive Collapse Analysis and Design Guidelines for New Federal Office Buildings and Major Modernization Projects. Washington, D.C; 2003.

[2] Department of Defense: Design of buildings to resist progressive collapse. Washington, D.C: UFC 4-023-03; 2009.

[3] Ellingwood BR, Smilowitz R, Dusenberry DO, Duthinh D, Lew HS, Carino NJ. Best Practices for Reducing the Potential for Progressive Collapse in Buildings. Rep. No. NISTIR 7396, National Institute of Standards and Technology, Maryland; 2007.

[4] Brett C, Lu Y. Assessment of robustness of structures: current state of research [J]. Frontiers of

Structural and Civil Engineering, 2013, 7(4): 1-13.

[5] Stylianidis P, Nethercot DA. Connection Modelling for Progressive Collapse Analysis. Proceeding of the 9th International Conference on Steel-Concrete Composite and Hybrid Structures. Leeds: Research Publishing; 2009.

[6] Sasani M, Kropelnicki J. Progressive Collapse Analysis of an RC Structure. Structural Design of Tall and Special Buildings 2008; 17(4): 757-771.

[7] Karns J, Houghton D, Hong J, Kim, J. Behaviour of Varied Steel Frame Connection Types Subjected to Air Blast, Debris Impact, and/or Post-Blast Progressive Collapse Load Conditions. Structures Congress 2009:1-10.

[8] Sadek F, Main JA, Lew HS, Bao Y. Testing and Analysis of Steel and Concrete Beam-to-column Assemblies under a Column Removal Scenario. Journal of Structural Engineering, ASCE 2011; 137(9): 881-892.

[9] Demonceau JF, Jaspart JP. Experimental Test Simulating a Column Loss in a Composite Frame. Advanced Steel Construction 2010; 6(3):891-913.

[10] Kozlowski A, Gizejowski M, Sleczka L, Pisarek Z, Saleh B. Experimental investigations of the joint behavior-Robustness assessment of steel and steel-concrete composite frame. In: Nunai L, Iványi M, Jármai K, editors. Proceeding of 6th Conference on Steel and Composite Structures. Hungary; 2011.

[11] Yi W, He Q, Xiao Y, et al. Experimental study on progressive collapse-resistant behavior of reinforced concrete frame structures. ACI Structural Journal 2008; 105(4): 433-439.

[12] Sadek F, Main JA, Lew HS, Robert SD, Chiarito VP, El-Tawil S. An Experimental and Computational Study of Steel Moment Connections under a Column Removal Scenario. Rep. No. NIST Technical Note 1669, National Institute of Standards and Technology, Maryland; 2010.

[13] Lee C, Kim S, Lee K. Parallel Axial-Flexural Hinge Model for Nonlinear Dynamic Progressive Collapse Analysis of Welded Steel Moment Frames. Journal of Structural Engineering, ASCE 2010, 136(2): 165-173.

[14] Yang B, Tan K H. Robustness of Bolted-Angle Connections against Progressive Collapse: Experimental Tests of Beam-Column Joints and Development of Component-Based Models. Journal of Structural Engineering, 2012, 139(9): 1498-1514.

[15] Yang B, Tan K H. Experimental tests of different types of bolted steel beam–column joints under a central-column-removal scenario. Engineering Structures, 2013, 54(0): 112-130.

[16] Liu Y, Málaga-Chuquitaype C, Elghazouli AY. Response of beam-to-column angle connections subjected to combined flexural and axial loading. In: Gardner L, editors. Proceeding of the 14th International Symposium on Tubular Structures. London; 2012

[17] Li L, Wang W, Chen YY, Lu Y. Experimental Investigation of Beam-to-Tubular Column Moment

Connections under Column Removal Scenario. Journal of Constructional Steel Research, 2013, 88: 244-255.

[18] Ministry of Construction of China: Code for design of steel structures . Beijing: 50017-2003; 2003.

[19] Ministry of Construction of China: Code for seismic design of buildings . Beijing: 50011-2010; 2010.

[20].Elremaily A, Azizinamini A, Experimental behavior of steel beam to CFT column connections. Journal of Constructional Steel Research, 2001. 57(10): 1099-1119.

[21] Technical specification for structures with concrete-filled rectangular steel tube members. CECS 159:2004.

[22] Architecture Institute of Japan: Techanical Recommendations for Steel Construction for Buildings -Part1 Guide to Steel-rib Fabrications. Toyko; 1996.

[23] Ministry of Construction of China: Code for design, construction and acceptance of high strength bolting for steel structure. Beijing: JGJ 82-91;1992.

[24] ABAQUS Analysis user's manual version 6.7. ABAQUS Inc.; 2007

List of figures

Table 1. Geometrical characteristics of specimens (dimensions in mm).

Specimen	Column section $D\times T$	Beam section $H\times B\times t_w\times t_f$	Inner-diaphragm $t=t_f$	Bolt layout at the beam web
SI-WB	SHS250×14	H300×150×6×8	8	4×1
SI-WB-2	SHS250×14	H300×150×6×8	8	2×2

Table 2. Material properties of specimens.

Components	Yield strength f_y (MPa)	Tensile strength f_u (MPa)	Elongation δ (%)
Plate of SHS250×14	411	653	28
Corner of SHS 250×14	414	748	32
Beam flange (t_f=8mm)	401	668	31
Beam web (t_w=6mm)	407	638	31

Table 3. Deformation limits and corresponding vertical loads

Specimen	Characteristic deflection limits		
	1st peak	2nd peak	Ultimate state
SI-WB	234mm (θ = 0.104 rad) 275 kN (1.53F_p)		≥ 345mm (θ = 0.153 rad) ≥ 307 kN (1.71F_p)
SI-WB-2	137 mm (θ = 0.061 rad) 207 kN (1.15F_p)	243 mm (θ = 0.108 rad) 226 kN (1.26F_p)	≥ 387 mm (θ = 0.170 rad) ≥ 232 kN (1.29F_p)

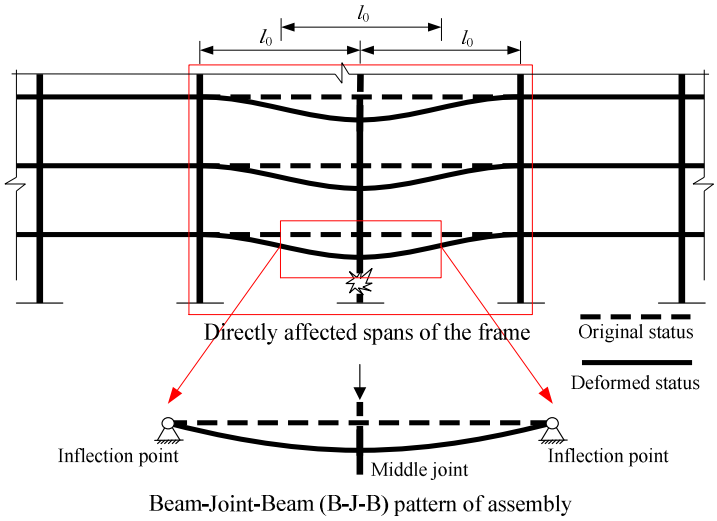

Fig. 1. A Beam-Joint-Beam assembly extracted from a framed structure.

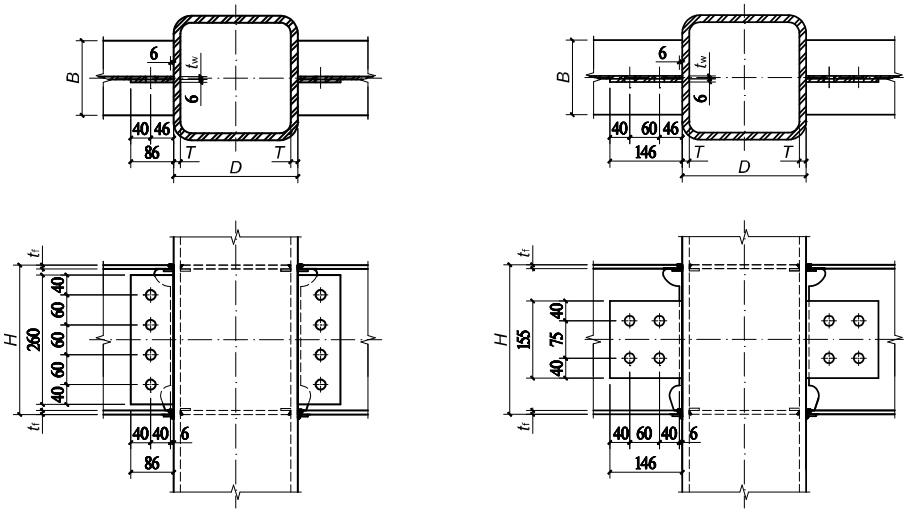

(a) Specimen SI-WB (b) Specimen SI-WB-2

Fig. 2. Details of the WUF-B moment connections with two different bolt layouts (dimensions in mm).

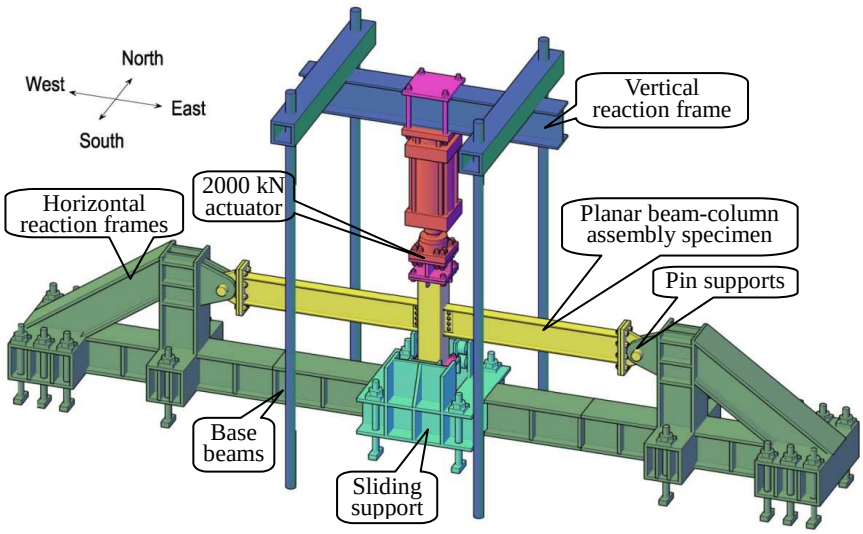

Fig. 3. Test setup.

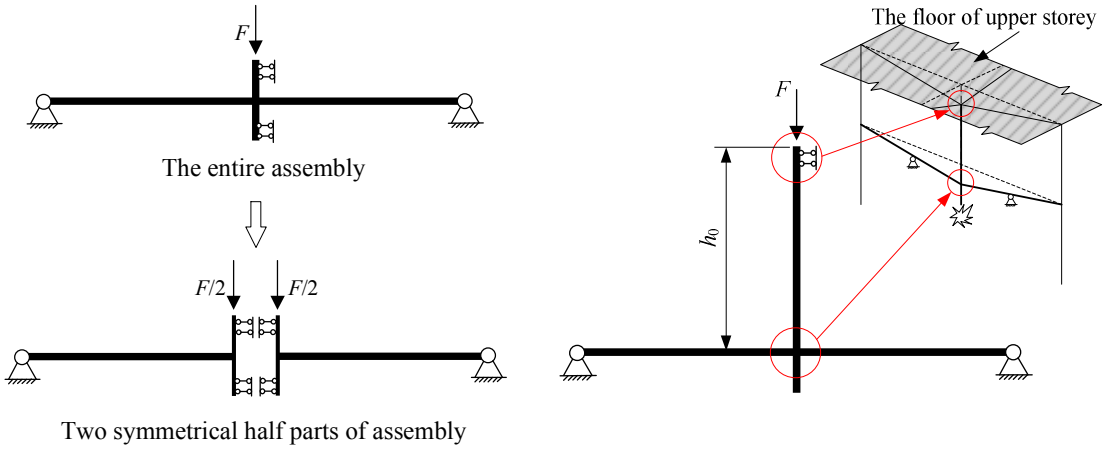

(a) The specimen assembly in tests (b) An assembly in an actual building

Fig. 4. The boundary conditions of the beam-to-column assembly.

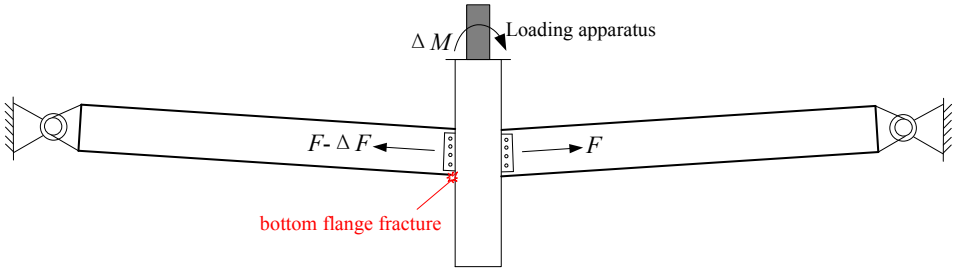

Fig. 5. Additional moment at the top of the column (without the sliding support).

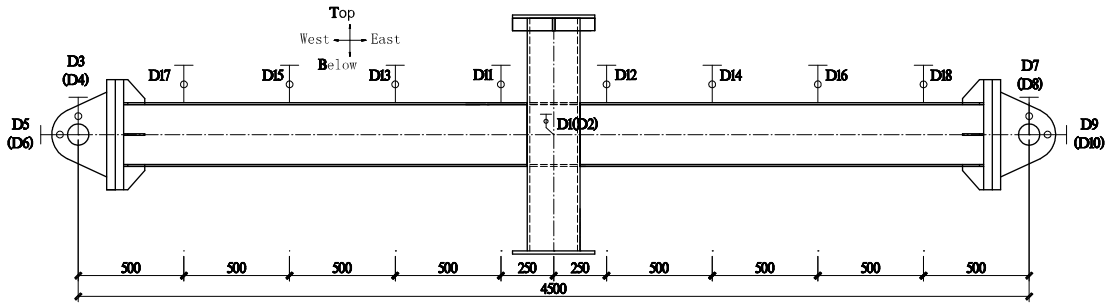

(a) Arrangement of displacement transducers.

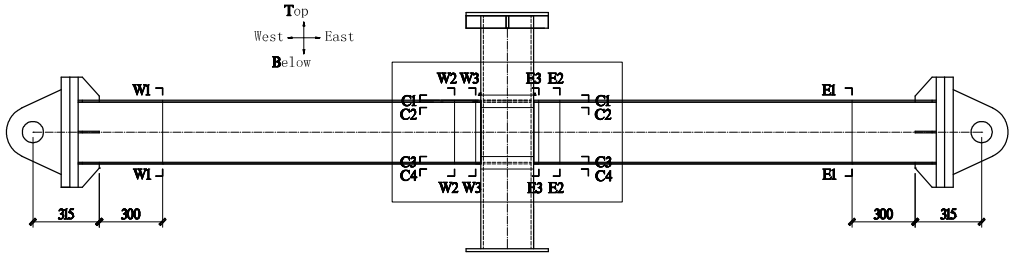

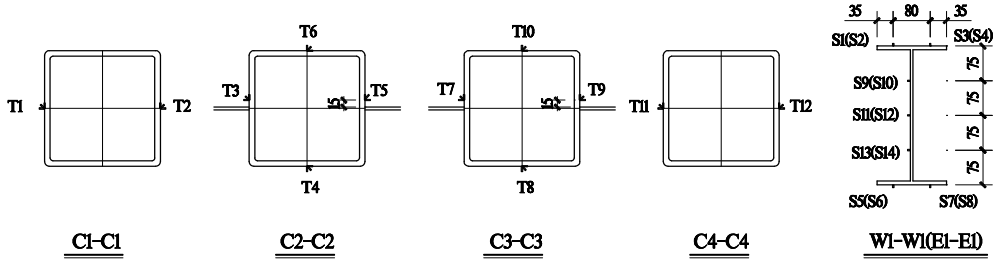

(b) Arrangement of strain gauges.

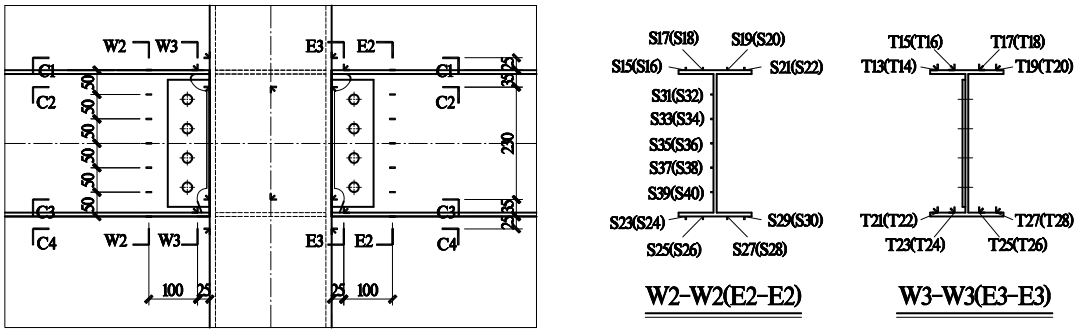

(c) Strain gauges in the joint region of Specimen SI-WB.

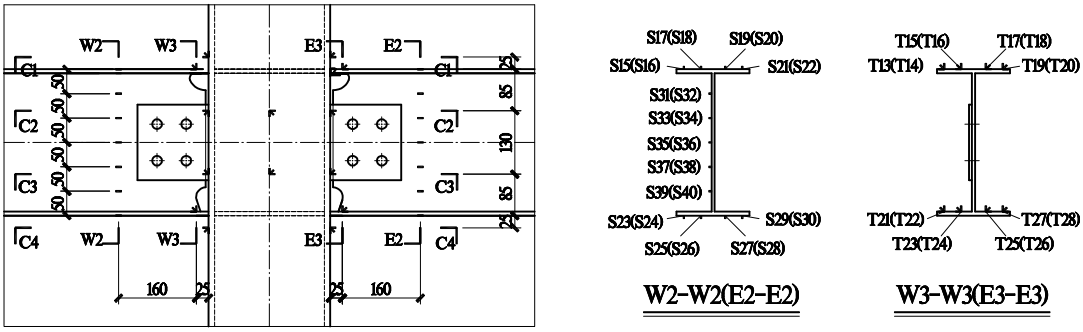

(d) Strain gauges in the joint region of Specimen SI-WB-2.

Fig. 6. Schematic of arrangements of displacement transducers and strain gauges.

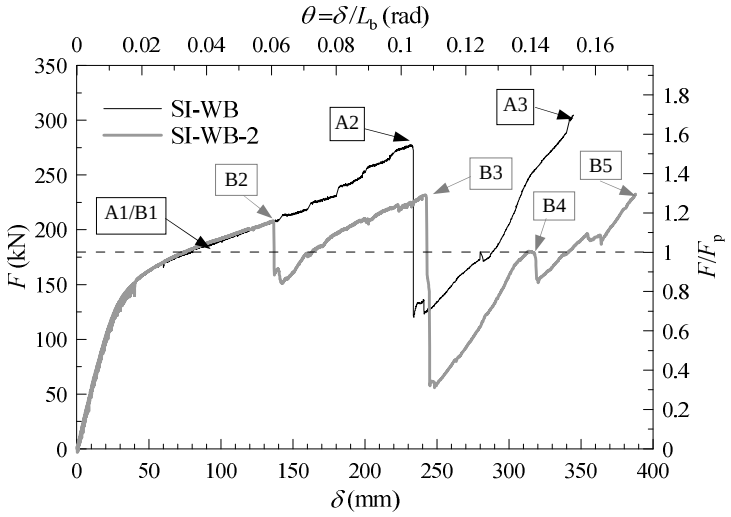

Fig. 7. Vertical load vs. displacement relationships of two specimens.

A1: Local buckling of top flanges near Section W3 and E3

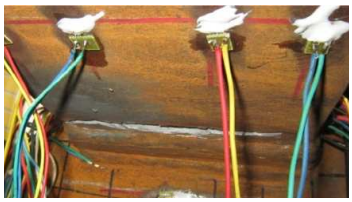

A2: Bottom flange fractured at Section E3 (1.54F_p, 0.104 rad)

A3: The lowest bolt was torn out of web at Section E3 (1.70F_p, 0.153 rad)

(a) Specimen SI-WB.

B1: Local buckling of top flanges near Section W3

B2: Column wall cracked near the bottom flange on the west side (1.15F_p, 0.061 rad)

B3: Bottom flange fractured at Section E3 (1.26F_p, 0.108 rad)

B4: Column wall completely fractured near the bottom flange on the west side (1.00F_p, 0.140 rad)

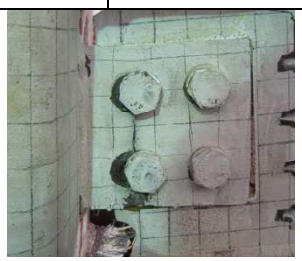

B5：Shear tab fractured at the inside section across the bolt holes (1.29F_p, 0.170 rad)

(b) Specimen SI-WB-2.

Fig. 8. Development of damage at key stages of response of the specimens.

Fig. 9. Separation between the bottom inner-diaphragm and column wall on the west side in Specimen SI-WB-2.

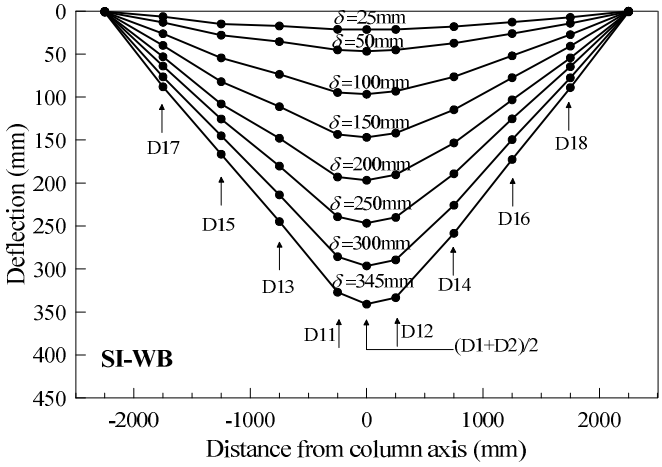

Fig. 10. Deflection profiles of specimen SI-WB.

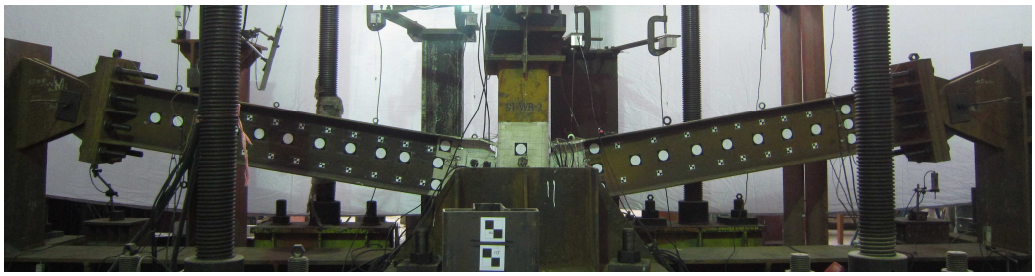

Fig. 11. Photograph of Specimen SI-WB-2 at the end of the test.

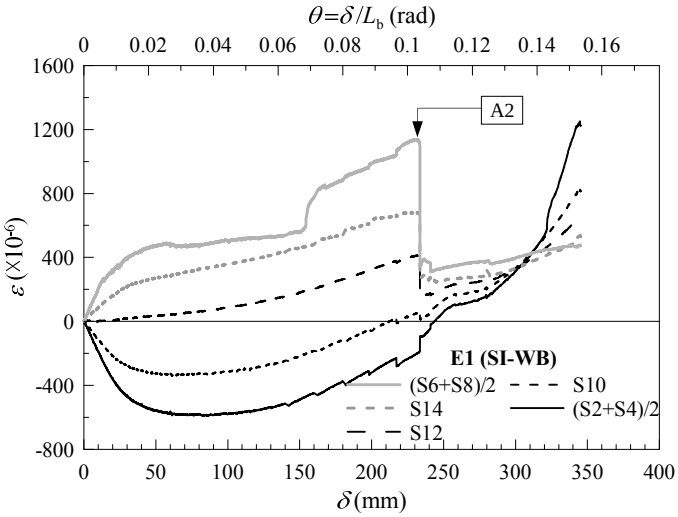

(a) Specimen SI-WB.

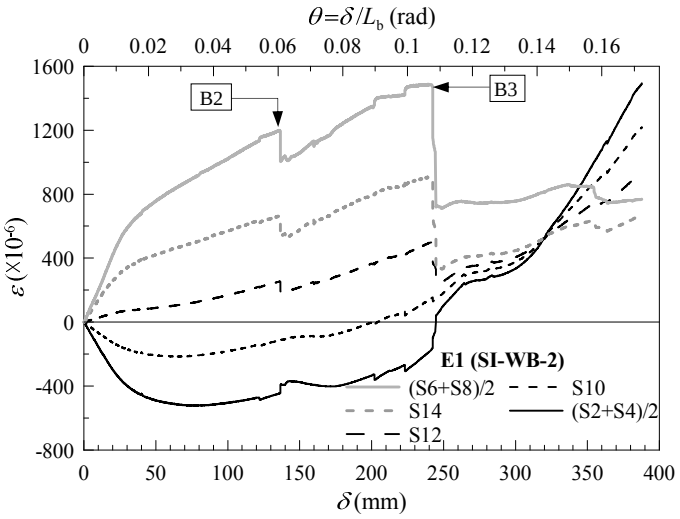

(b) Specimen SI-WB-2.

Fig. 12. Strain development at the elastic Sections E1 of two specimens.

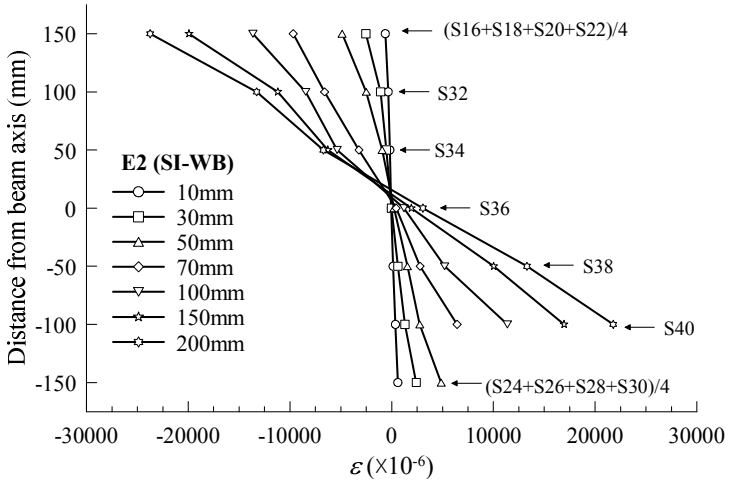

(a) Specimen SI-WB.

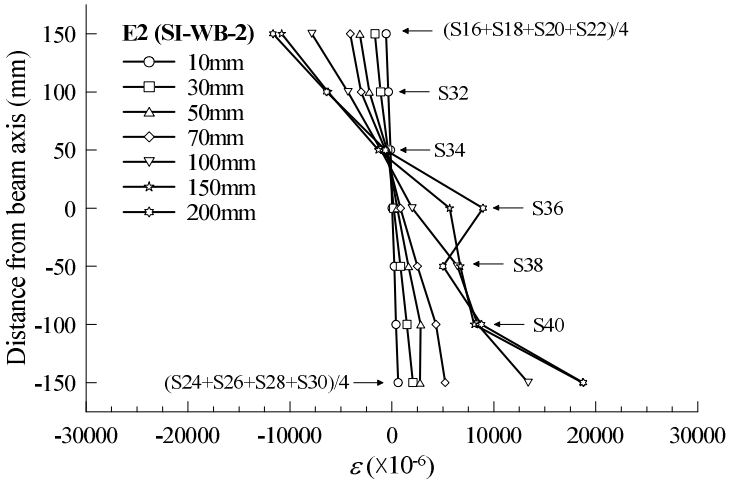

(b) Specimen SI-WB-2.

Fig. 13. Strain distributions at Section E2 before bottom flange fracture at Section E3.

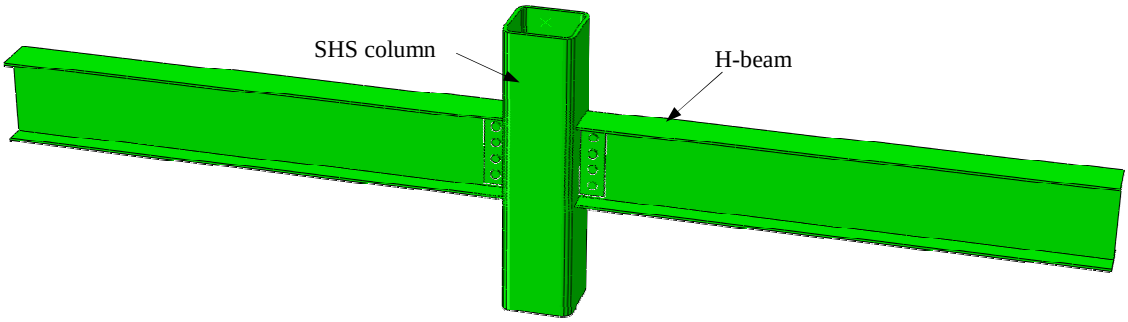

(a) Overview of the FE models for beam-to-column assembly

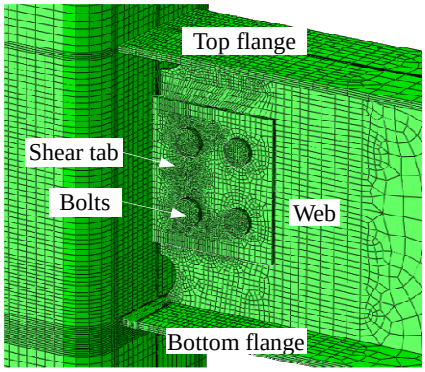

(b) Detailed view of connection zone in Specimen SI-WB

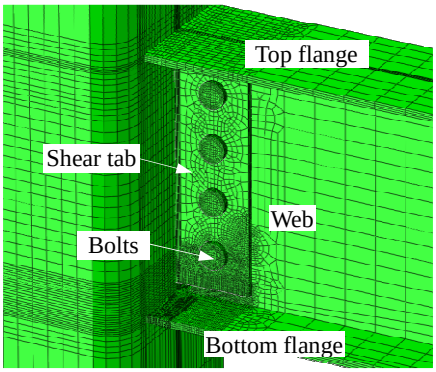

(c) Detailed view of connection zone in Specimen SI-WB-2

Fig. 14. Finite element models of two specimens

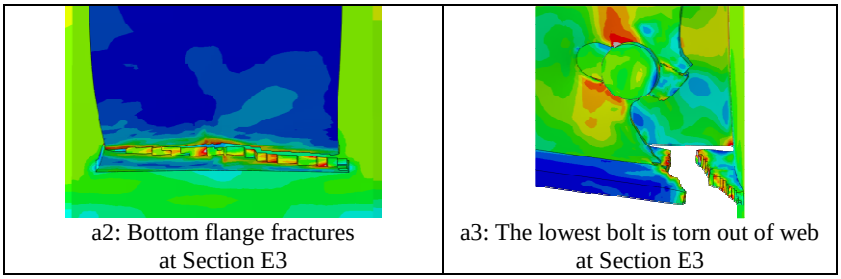

(a) Specimen SI-WB

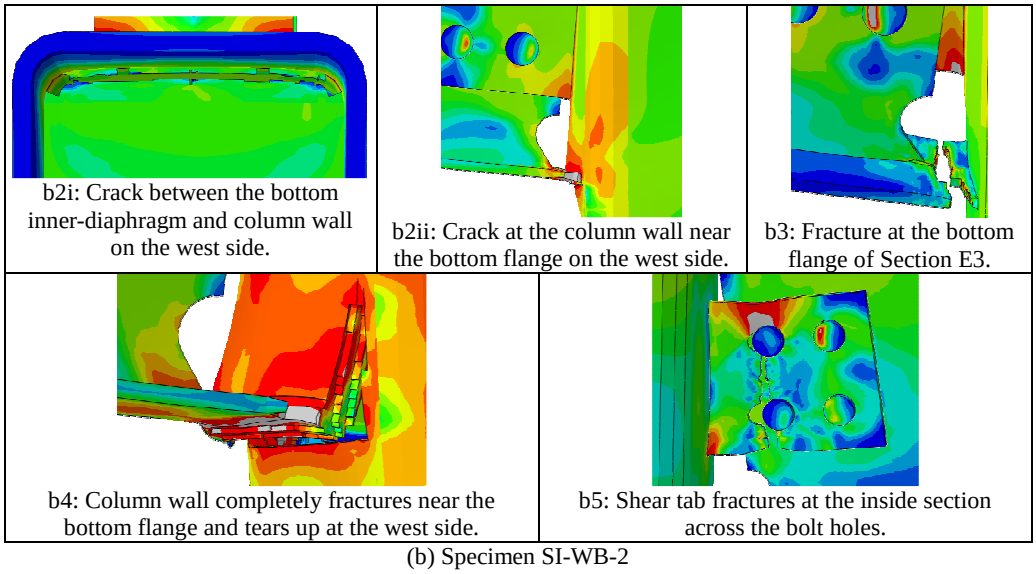

(b) Specimen SI-WB-2

Fig. 15. Failure modes of two specimens in the FE simulation

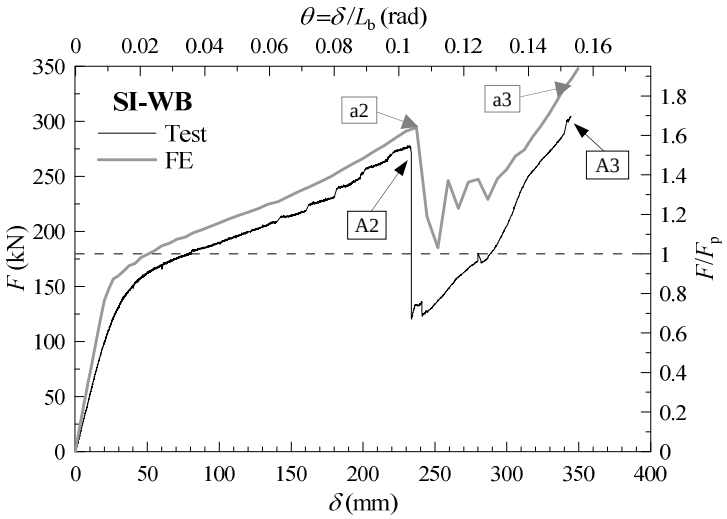

(a) Specimen SI-WB

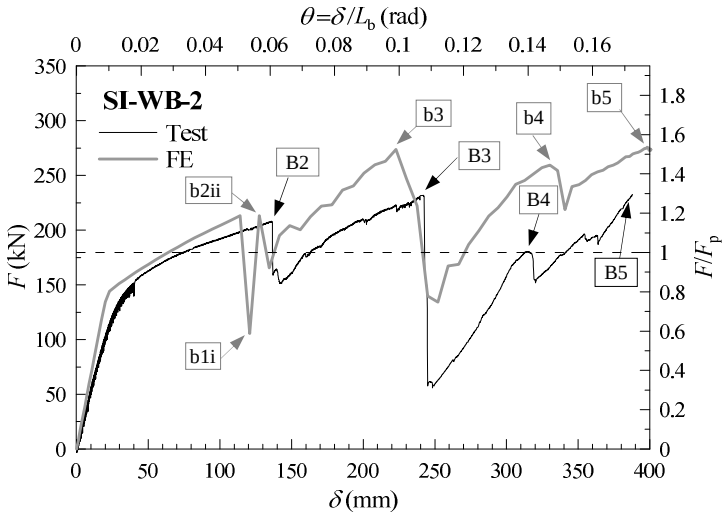

(b) Specimen SI-WB-2

Fig. 16. Vertical load vs. displacement relationships comparison between numerical simulations and tests.

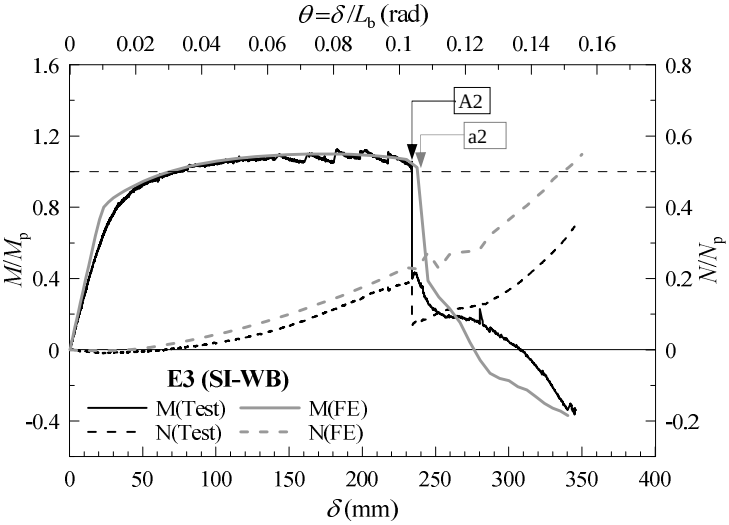

(a) Specimen SI-WB

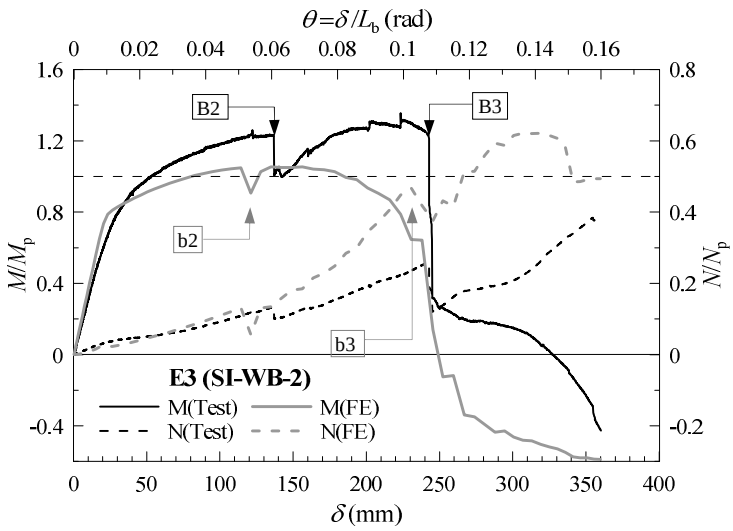

(b) Specimen SI-WB-2

Fig. 17. The development of bending moment and axial force of Section E3.

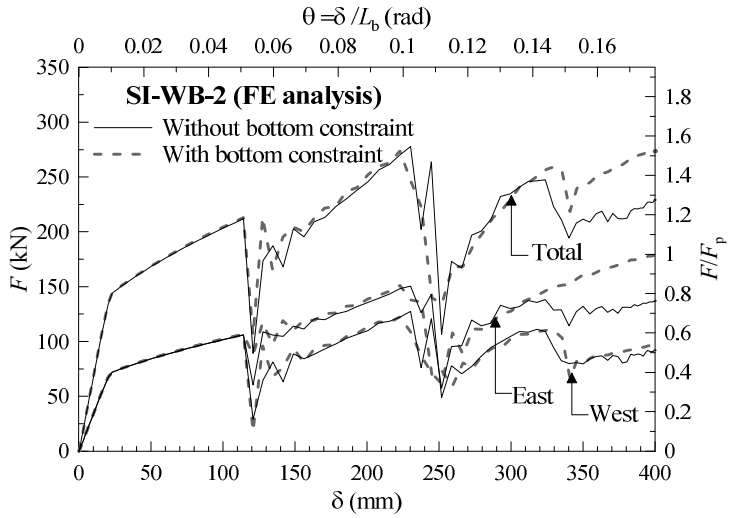

Fig. 18. Vertical resistance comparison between the assembly models with or without the constraints at the column bottom

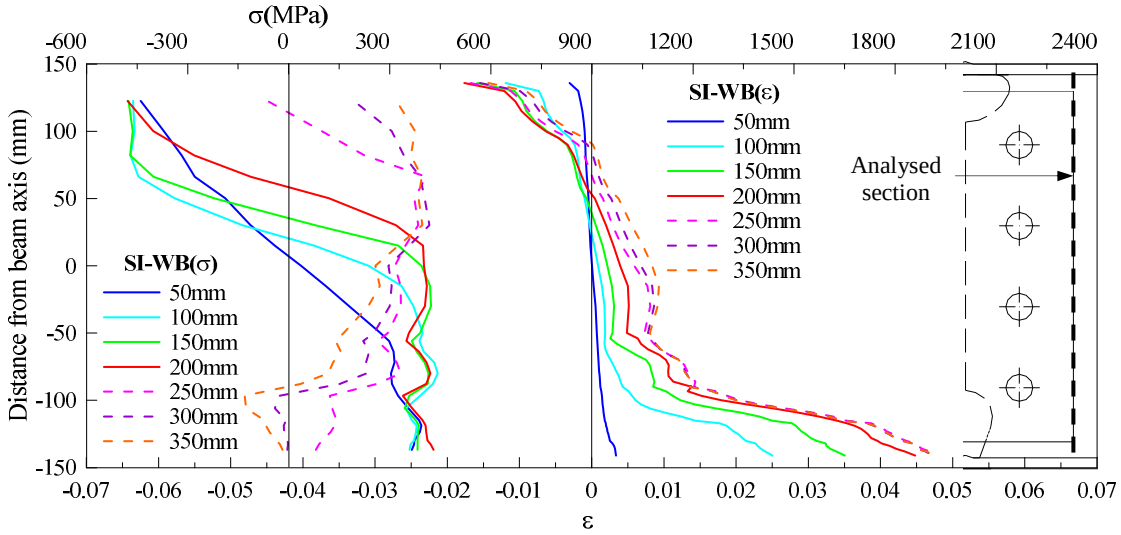

(a) Specimen SI-WB

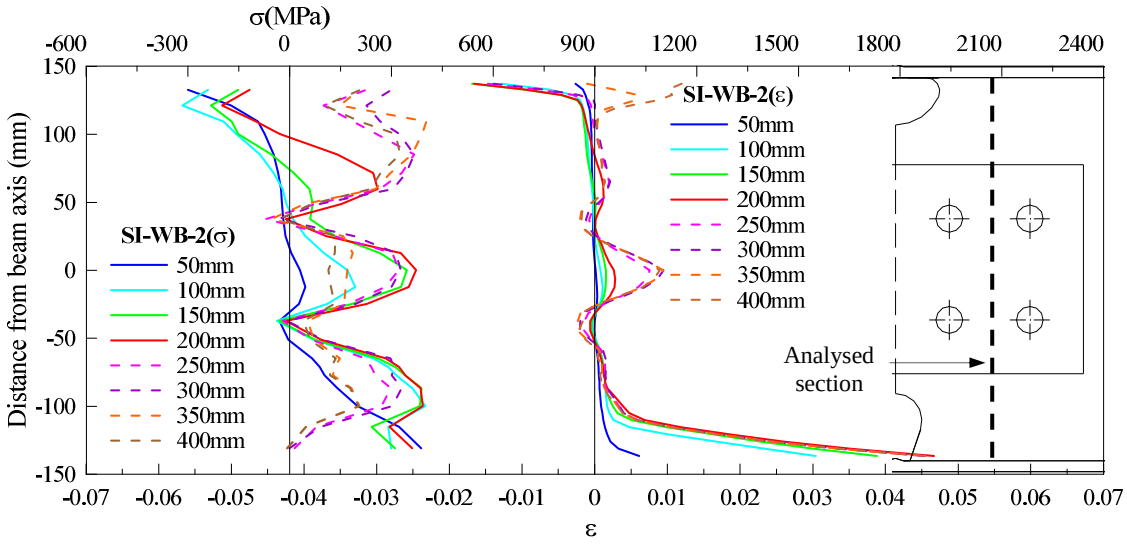

(b) Specimen SI-WB-2

Fig. 19. Stress (σ) and strain (ε) distributions at the bolted web in the vicinity of the connection

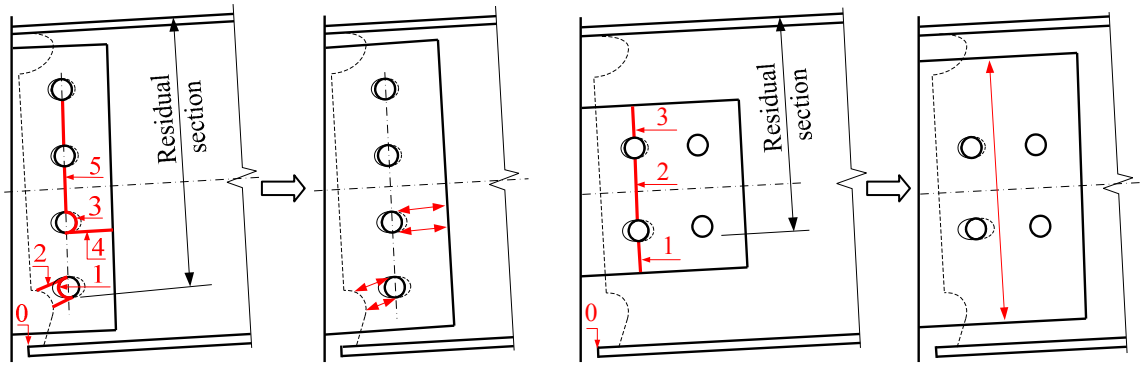

(a) Specimen SI-WB and improvement scheme

(b) Specimen SI-WB-2 and improvement scheme

Fig. 20. Potential failure modes and their sequences of the bolted web in the WUF-B connection

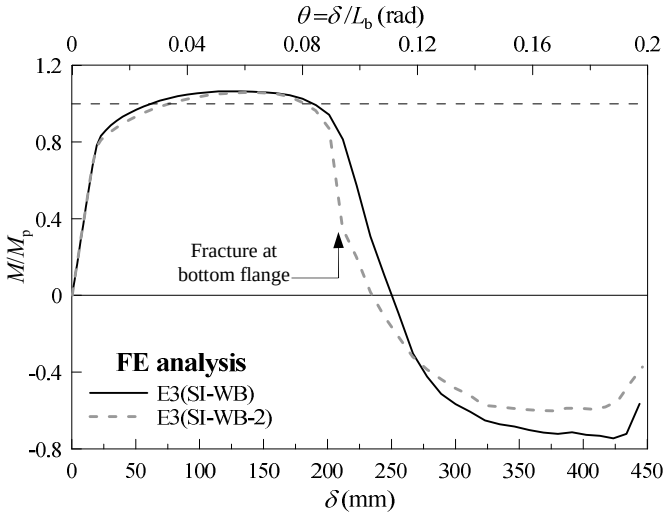

(a) Bending moment.

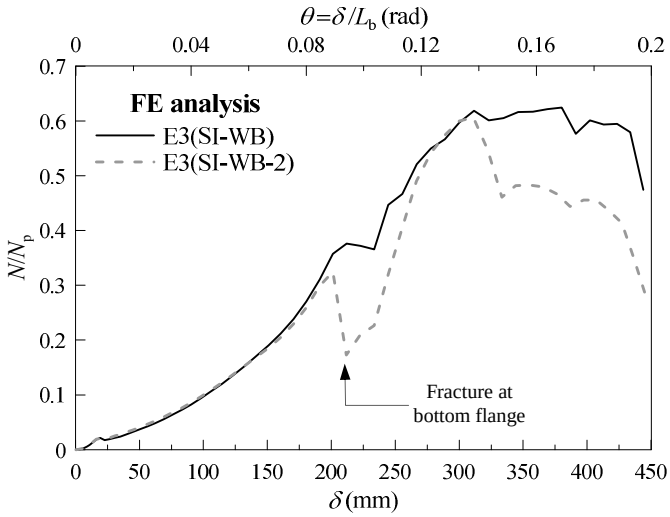

(b) Axial tension

Fig. 21. Development of bending moment and axial tension at critical sections

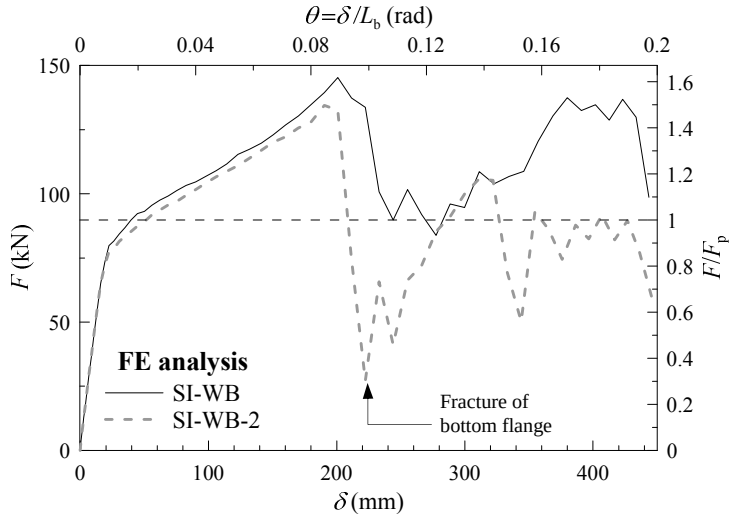

Fig. 22. Vertical resistance vs displacement in two half-assemblies into final failure